A warm ultraluminous infrared galaxy just 600 million years after the big bang

Downloaded from: https://research.chalmers.se, 2025-12-05 06:15 UTC

Citation for the original published paper (version of record):
Bakx, T., Sommovigo, L., Tamura, Y. et al (2025). A warm ultraluminous infrared galaxy just 600 million years after the big bang. Monthly Notices of the Royal Astronomical Society, 544(2): 1502-1513. http://dx.doi.org/10.1093/mnras/staf1714

N.B. When citing this work, cite the original published paper.

research.chalmers.se offers the possibility of retrieving research publications produced at Chalmers University of Technology. It covers all kind of research output: articles, dissertations, conference papers, reports etc. since 2004. research.chalmers.se is administrated and maintained by Chalmers Library

(article starts on next page)

Monthly Notices of the ROYAL ASTRONOMICAL SOCIETY
MNRAS **544,** 1502–1513 (2025) https://doi.org/10.1093/mnras/staf1714

A warm ultraluminous infrared galaxy just 600 million years after the big bang

T. J. L. C. Bakx [1,1★] Laura Sommovigo [2] Yoichi Tamura [3] Renske Smit,[4] Andrea Ferrara,[5] Hiddo Algera [6] Susanne Aalto,[1] Duncan Bossion [7] Stefano Carniani [5] Clarke Esmerian,[1] Masato Hagimoto [3] Takuya Hashimoto [8,9] Bunyo Hatsukade,[10,11,12] Edo Ibar,[13,14] Hanae Inami [15] Akio K. Inoue [16,17] Kirsten Knudsen [1] Nicolas Laporte [18] Ken Mawatari,[17,19] Juan Molina [13,14] Gunnar Nyman [20] Takashi Okamoto,[21] Andrea Pallottini [5,22] W. M. C. Sameera,[1] Hideki Umehata,[3,23] Wouter Vlemmings[1] and Naoki Yoshida[12]

Affiliations are listed at the end of the paper

Accepted 2025 October 4. Received 2025 September 30; in original form 2025 August 15

ABSTRACT

We present an Atacama Large Millimeter/submillimeter Array (ALMA) Band 9 continuum detection (3.3σ) of MACS0416_Y1 that confirms the suspected warm dust (91^{+62}_{-35} K) of this Lyman-Break Galaxy (LBG) at $z = 8.3$ with $\log_{10} M_*/\mathrm{M}_\odot = 9.0 \pm 0.1$. A modified blackbody fit to the ALMA Bands 3 through 9 data of MACS0416_Y1 finds an intrinsic infrared luminosity of $1.0^{+1.8}_{-0.6} \times 10^{12}$ $\mathrm{L}_\odot$, placing this UV-selected LBG in the regime of Ultra Luminous Infrared Galaxies. Its luminous but modest dust reservoir ($1.4^{+1.3}_{-0.5} \times 10^6$ $\mathrm{M}_\odot$) is cospatial to regions with a UV-continuum slope $\beta_{\mathrm{UV}} \approx -1.5$ as seen by *James Webb Space Telescope* (*JWST*) imaging. Although this implies some dust obscuration, the *JWST* photometry implies less obscured star formation than seen in the complete characterization by ALMA, implying some spatial separation of dust and stars on scales below 200 pc, i.e. smaller than those probed by *JWST* and ALMA. This source is an extreme example of dust-obscured star formation contributing strongly to the cosmic build-up of stellar mass, which can only be revealed through direct and comprehensive observations in the (sub)mm regime.

Key words: galaxies: evolution – galaxies: formation – galaxies: high-redshift – dust, extinction – infrared: galaxies – submillimetre: galaxies.

1 INTRODUCTION

Observations with the Atacama Large Millimeter/submillimeter Array (ALMA) have revealed the presence of dust in galaxies in the epoch of reionization (e.g. D. Watson et al. 2015; Y. Tamura et al. 2019; T. J. L. C. Bakx et al. 2020b; Y. Fudamoto et al. 2021; H. Inami et al. 2022; Y. Tamura et al. 2023; H. S. B. Algera et al. 2024a). This was somewhat surprising, since ultraviolet (UV) studies that map out the unobscured star-formation rate density (SFRD) to $z \sim 10$ suggested a lack of dust at the high-redshift end based on the blue UV slopes of low stellar mass high-z galaxies (β_{UV}; e.g. R. J. Bouwens et al. 2015; S. L. Finkelstein et al. 2015; A. Saxena et al. 2024; A. Ferrara et al. 2025). Although the *James Webb Space Telescope* (*JWST*) is finding reddened UV-slopes in the $z > 8$ Universe (e.g. D. Langeroodi et al. 2024), uncertainties still remain regarding the fraction of and extent of dust-obscured star formation in the early Universe because of the lack of comprehensive $z \gtrsim 8$ dust emission studies. These high-redshift studies are inherently challenging, as they demand substantial observational time even for single-band detections; yet constructing reliable spectral energy distributions (SEDs) requires multiband coverage. Regardless of strategy, such surveys remain biased towards the brightest sources (A. K. Inoue et al. 2016; T. Hashimoto et al. 2019) or gravitationally lensed objects (D. Watson et al. 2015; K. K. Knudsen et al. 2017; T. J. L. C. Bakx et al. 2021; H. B. Akins et al. 2022; S. Fujimoto et al. 2024), typically those pre-selected in the ultraviolet (c.f., T. J. L. C. Bakx et al. 2024).

Initially, the strong far-infrared emission at $z > 7$ revealed by ALMA observations was attributed to the presence of unexpectedly large dust masses in the observed high-z galaxies (A. Leśniewska & M. J. Michałowski 2019; F. Pozzi et al. 2021). This exciting indication of rapid dust accumulation in the early Universe has guided studies into the physics of grain production and processing in the interstellar medium (ISM) in the early Universe (e.g. C. R. Choban et al. 2022, 2024; A. Ferrara, A. Pallottini & P. Dayal 2023; H. Hirashita & C.-C. Chen 2023; D. Narayanan et al. 2025). However, these constraints require accurate dust mass measurements (see e.g. A. K. Inoue et al. 2020; L. Sommovigo et al. 2020; C. J. Esmerian & N. Y. Gnedin 2024), as they strongly depend on the dust temperature and instead most measurements currently resort to using an ad hoc temperature instead ($T_{\mathrm{d}} \sim 35 - 50$ K; e.g. R. Bouwens et al. 2020).

★ E-mail: tom.bakx@chalmers.se

© The Author(s) 2025.
Published by Oxford University Press on behalf of Royal Astronomical Society. This is an Open Access article distributed under the terms of the Creative Commons Attribution License (https://creativecommons.org/licenses/by/4.0/), which permits unrestricted reuse, distribution, and reproduction in any medium, provided the original work is properly cited.

Downloaded from https://academic.oup.com/mnras/article/544/2/1502/8318242 by guest on 21 November 2025

Both recent observations (e.g. D. Schaerer et al. 2015; A. L. Faisst et al. 2017; N. Laporte et al. 2019; T. J. L. C. Bakx et al. 2020b; M. P. Viero et al. 2022; J. Witstok et al. 2023a) and theoretical studies (e.g. L. Sommovigo et al. 2020, 2021) indicate that this ad hoc approach to dust temperatures might not be appropriate to study dust-obscured star formation in the early Universe, as dust temperatures between galaxies can vary strongly, affecting the estimated dust masses and obscured star-formation rates (C. Behrens et al. 2018). Observationally, two galaxies at $z > 7.5$ have deep dust upper limits at ~ 160 μm that contrast against bright ~ 90 μm emission, indicating the presence of warm dust in these optically selected galaxies ($T_{\rm d} \gg 60$ K; N. Laporte et al. 2019; T. J. L. C. Bakx et al. 2020b). Such high temperatures can alleviate the large dust mass requirements set by the observed infrared emission (A. Leśniewska & M. J. Michałowski 2019; L. Sommovigo et al. 2020). This dust-temperature dependence is very strong indeed, affecting the dust mass and dust-obscured star-formation rate estimates by the sixth power, as the luminosity scales as $T_{\rm d}^{4+\beta_{\rm d}}$, where $\beta_{\rm d} \sim 2.0$.

While rest-frame UV to near-infrared dust studies at high redshift find evidence of dust through dust attenuation slopes (V. Markov et al. 2023, 2025; R. Fisher et al. 2025), extinction bumps (J. Witstok et al. 2023b), and polyaromatic hydrocarbons (J. S. Spilker et al. 2023), the properties of this dust in the early Universe might be very different to those observed in local galaxies (c.f. L. Sommovigo et al. 2025). Instead, (sub)mm studies with ALMA have revealed a tendency towards the measurement of higher $\beta_{\rm d}$ in galaxies (Y. Kato et al. 2018; J. Witstok et al. 2023a; H. S. B. Algera et al. 2024b) and quasars (R. Tripodi et al. 2023). On top of the well-understood effects of the cosmic microwave background radiation, which both heats the dust and reduces the contrast against which we observe the dust (E. da Cunha et al. 2013), the emissive properties of dust grains at $z > 7$ appear to contrast against the picture painted by recent *JWST* observations. Alternative to – or together with – a high-dust temperature, galaxies in the early Universe show a variety of dust attenuation curves (V. Markov et al. 2023, 2025; R. Fisher et al. 2025) resulting from different compositions (K. Demyk et al. 2017a, b) or size distributions (A. Ferrara et al. 2017; J. McKinney et al. 2025; D. Narayanan et al. 2025), perhaps influenced by grain coagulation or icy mantles on the surface of grains, particularly in the denser regions of the ISM (see the discussion in M. W. L. Smith et al. 2017).

A comprehensive characterization of the dust emission of distant galaxies is key to understanding their role within galaxy evolution. In an effort to characterize the formation of stars across cosmic time, the discrepancy between the obscured and unobscured cosmic SFRD in the $z > 5$ Universe has become ever more egregious (e.g. M. Novak et al. 2017; C. Gruppioni et al. 2020; M. Talia et al. 2021). Particularly, the galaxies that dominate the sub-mm emission at cosmic noon ($z = 1 - 5$) are not yet abundant enough in the cosmic dawn, adding additional uncertainty to the high-redshift cosmic SFRD. A population of low-metallicity, young galaxies with small but warm dust reservoirs could dominate the cosmic SFRD (L. Sommovigo et al. 2022a), where even a small amount of dust is sufficient to obscure most of the galaxy. Such galaxies would be missed in studies that focus on ∼0.8–2 mm detected galaxies, even from deep fields conducted with ALMA (J. A. Zavala et al. 2021), and could alleviate the discrepancy in cosmic star-formation rate estimates (M. P. Viero et al. 2022).

The galaxy at the centre of this study, MACS0416_Y1 (Y1 hereafter, located at the IRCS coordinates 04:16:09.401, −24:05:35.47), could be an archetypal example of a low-metallicity galaxy with a small but warm dust component. Y1 is a $z = 8.31$ Lyman-break galaxy (LBG) with both robust [O III] 88 μm and [C II] 158 μm line detections as well as a resolved dust continuum detection at a resolution of 300 parsec. The source was originally identified as a $z \approx 8$ bright ($H_{160} = 25.9$) LBG behind the *Hubble* Frontier Field cluster MACS J0416.1−2403. Y1 is moderately magnified ($\mu_{\rm g} = 1.5$, R. Kawamata et al. 2016; G. Rihtaršič et al. 2024) with negligible differential lensing. The spectroscopic redshift was initially identified using the [O III] 88 μm line (Y. Tamura et al. 2019). The dust continuum at 90 μm, adjacent to the [O III], was clearly detected at $> 5\sigma$. However, subsequent attempts to reveal the dust continuum at longer wavelengths did not detect any emission around the [C II] 158 μm line (T. J. L. C. Bakx et al. 2020b). These deep observations provide a strict upper limit at 160 μm, and indicate that the 90 μm continuum detection still lies on the Rayleigh–Jeans part of the slope of the modified blackbody emission, with a dust temperature in excess of ~ 80 K.

Only high-frequency observations, probing close to or on the other side of the peak of the dust spectrum, can conclusively measure the dust temperature of a galaxy (e.g. T. J. L. C. Bakx et al. 2021; H. S. B. Algera et al. 2024b). A study of the dust temperature using Band 8 at 70 μm finds a 3.5σ detection at 254 ± 81 μJy (A. Harshan et al. 2024), but did not probe close enough to the peak of the spectrum to put a lower bound on the dust temperature. This paper presents the high-frequency continuum measurements that are finally able to constrain the dust temperature in Y1. Combined with previous sub-mm results (Section 2), we provide a detailed analysis of the dust spectrum (Section 3) to investigate the properties of the furthest direct detection of dust emission in the Universe (Section 4). We provide the conclusions in Section 5.[1]

2 OBSERVATIONS

Using ALMA Band 9 (A. M. Baryshev et al. 2015) observations at 671 GHz, we aim to measure the dust temperature of Y1 by characterizing its short-wavelength dust emission. Band 9, and specifically the 671 GHz window, provides the optimum frequency to measure Y1's likely warm dust temperature, with a more extensive justification given in Appendix A. In total, four observations accumulate a total of 4.9 h including overheads between November 9th and December 20th 2024 in the compact configurations C43-1, C43-2, and C43-3 with baseline lengths between 14 and 500 m (see Appendix Table A1). Two quasars, J0348–2749 and J0519-4546, were used for complex gain calibration, and another quasar, J0423−0120, was used for bandpass calibration. The data were calibrated using the pipeline script provided.

The continuum image is produced with CASA pipeline version 6.5.4.9 (J. P. McMullin et al. 2007; CASA Team et al. 2022) using natural weighting to extract the continuum flux with the highest significance. The dust continuum emission is seen extended across 1.5 beams at 2σ. In an effort to best extract the flux, we aim to extract the flux directly from the peak pixel using tapered imaging. This flux extraction method tends to be more robust against noise peaks than aperture-based curve-of-growth algorithms, especially when the signal-to-noise ratio of the data is modest, see (D. der Vlugt et al. 2021; H. S. B. Algera et al. 2024b). As such, we explore the total flux from the band 9 image through eleven different uv-tapering settings between 0 and 1 arcsec at 0.1 arcsec intervals. The total flux is estimated on each image through a curve-of-growth analysis, in

[1]Throughout this paper, we assume a flat Λ-Cold Dark Matter cosmology with the best-fitting parameters derived from the *Planck* results (Planck Collaboration VI 2020), which are $\Omega_{\rm m} = 0.315$, $\Omega_\Lambda = 0.685$ and $h = 0.674$.

Downloaded from https://academic.oup.com/mnras/article/544/2/1502/8318242 by guest on 21 November 2025

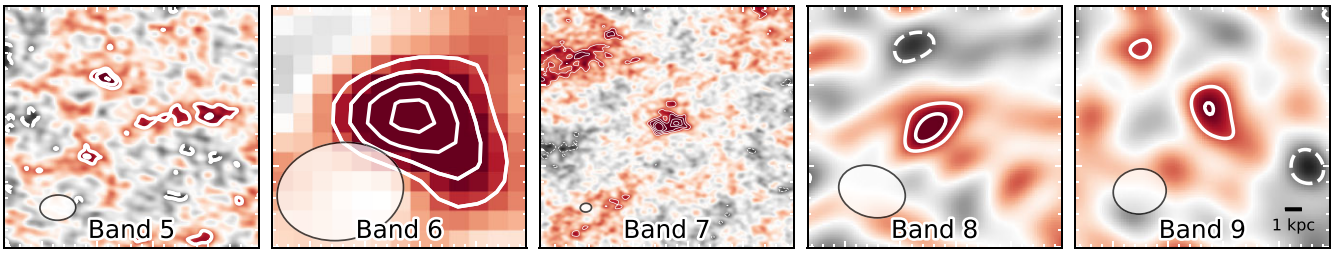

Figure 1. The dust continuum of MACS0416-Y1 in all (tentatively) detected Bands, namely 5, 6, 7, 8, and 9 – covering rest-frame wavelengths 160 to 45 μm. For Band 9, the 0.5 arcsec uv-tapered dust continuum is shown. The poststamps are 3 arcsec × 3 arcsec, with the background image showing the continuum overlaid, together with *white contours* indicating the 2, 3, 4, 5σ emission. The beam is shown in the bottom-left corner, and the scalebar is shown in the bottom-right corner in the right-hand side poststamp.

an effort to extract the total available flux with a sufficiently low total noise estimate. The signal strength plateaus at a tapering of 0.4 arcsec, indicating that the source remains unresolved at this and larger taper values. Fig. 1 shows the resulting tapered Band 9 image with a 0.66 arcsec × 0.57 arcsec beam with a position angle of 84 deg, with an r.m.s. level of 140 μJy beam^{-1} and a peak flux density of 465 ± 140 μJy (∼ 3.3σ). An additional 10 per cent flux calibration uncertainty is added in quadrature, based on the recommendations from the ALMA technical handbook.[2]

Additionally, deep Band 6 data was taken to search for the [O I] 146 μm emission (PID: 2024.1.00995.S; P.I. Renske Smit). The data are cleaned using the same procedure as described for the Band 9 data, i.e. using the pipeline script provided. Being a line detection experiment, the observations – at a central frequency of 226.8 GHz – were not designed to spatially resolve Y1. In imaging the Band 6 continuum emission of the source, we excluded channels potentially contaminated by the [O I] line, defined as those within ±191 km s^{-1} – the line full width at half-maximum of [C II] in T. J. L. C. Bakx, S. Eales & A. Amvrosiadis (2020a) – around a central redshift of z = 8.3116. Adopting natural weighting, the image attains a sensitivity of σ = 6.5 μJy beam^{-1}, and has a beam size of 1.6 arcsec × 1.2 arcsec. At this resolution, Y1 remains unresolved and we measure a peak flux density of 41.7 ± 6.5 μJy beam^{-1} (6.4σ).

The Band 4 data (2022.1.01356.S; P.I. Eiichi Egami) originates from an ALMA mapping observation. Using the online-reduced data from the ALMA science archive, we investigate the Band 4 emission at the position of Y1 using the primary-beam corrected continuum image. Y1 lies at the edge of the mapped region and remains undetected, with a primary-beam correction of 0.40. Using natural weighting, the 3σ flux limit is estimated to be < 340 μJy, with a beam size of 1.6 arcsec × 1.1 arcsec.

The flux measurements of Y1 in Bands 3 through 9, including those from several shallower surveys, are provided in Table 1.[3] The images of the Bands in which Y1 is (tentatively) detected are shown in Fig. 1. The higher resolution data yields a strong 137 μJy continuum detection at 90 μm, with only an 18 μJy upper limit at 3σ after substantial tapering (i.e. smoothing the image in the uv-plane) at 160 μm. Using uv-based flux extraction with UVMULTIFIT (I. Martí-Vidal et al. 2014), a total flux 12 ± 6 μJy is measured from the combined Band 5 data (Bakx et al. in prep.), in agreement with the flux limit of the tapered map. Based on the uv-based flux extraction of Band 5, we identify this emission as tentatively detected at 2σ. The subsequent analysis of fitting does not change appreciatively between a 2σ detection and a 3σ upper limit. All reported continuum fluxes are extracted from imaging that has been sufficiently tapered to leave the source unresolved.

Table 1. Continuum measurements and results from the SED fits for MACS0416-Y1.

	λ (mm)	$S_\nu^{\rm obs}$ (μJy)	Reference
Band 9/671 GHz	0.447	465 ± 147	This work
Band 8/465 GHz	0.645	254 ± 81	A. Harshan et al. (2024)
Band 7/353 GHz	0.849	137 ± 26	Y. Tamura et al. (2019, 2023)
Band 6/263 GHz	1.14	< 174 (3σ)	T. J. L. C. Bakx et al. (2020b)
Band 6/227 GHz	1.31	41.7 ± 6.5	This work
Band 5/197 GHz	1.52	12 ± 6	T. J. L. C. Bakx et al. (2020b) Bakx et al. in prep.
Band 4/143 GHz	2.09	< 340 (3σ)	This work
Band 3/ 93 GHz	3.23	< 21 (3σ)	G. C. Jones et al. (2024)
		SED fits	
$T_{\rm d}$ (K)	91^{+62}_{-35}	72^{+10}_{-9}	94^{+17}_{-14}
$\beta_{\rm d}$	$1.52^{+1.09}_{-0.75}$	2 (*fixed*)	1.5 (*fixed*)
$M_{\rm d}$ (10^6 M$_\odot$)[a]	$1.4^{+1.3}_{-0.5}$	$1.9^{+0.7}_{-0.5}$	$1.4^{+0.5}_{-0.4}$
$L_{\rm IR}$ [10^{12} L$_\odot$)[a]	$1.0^{+1.8}_{-0.6}$	$0.7^{+0.5}_{-0.3}$	$1.1^{+1.0}_{-0.5}$
$\log_{10}$ IRX	$1.4^{+0.5}_{-0.3}$	$1.3^{+0.3}_{-0.3}$	$1.4^{+0.4}_{-0.3}$
$M_{\rm d}$/SN (M$_\odot$)	$0.07^{+0.06}_{-0.03}$	$0.05^{+0.04}_{-0.03}$	$0.06^{+0.03}_{-0.02}$

[a]Corrected for the magnification assuming μ = 1.5 from R. Kawamata et al. (2016) and G. Rihtaršič et al. (2024), note that the listed fluxes are not corrected for lensing. Non-detections are listed in italics, while the uv-based extraction of the Band 5 is listed as a 2σ tentative detection.

3 FITTING OF THE SPECTRAL ENERGY DISTRIBUTION

Fig. 2 shows the modified blackbody (equation 8 in L. Sommovigo et al. 2021) fitted to the continuum points reported in Table 1. We use equations (12) and (18) from E. da Cunha et al. (2013) to account for the heating of dust by and decreasing contrast against the cosmic microwave background (CMB), respectively, with the $T_{{\rm CMB},z=8.3}$ = 25.4 K. We approximate the dust mass absorption coefficient (κ_ν) as $\kappa_\star\,(\nu/\nu_\star)^{\beta_{\rm d}}$, with ($\kappa_\star$, $\nu_\star$) as (10.41 cm^2 g^{-1}, 1900 GHz) from B. T. Draine (2003). We use the EMCEE MCMC-fitting routine (D. Foreman-Mackey et al. 2013), and allow $\log_{10} M_{\rm d}$, $T_{\rm d}$, and $\beta_{\rm d}$ to vary freely using flat priors, resulting in a dust mass of $1.4^{+1.3}_{-0.5} \times 10^6$ M$_\odot$, a

[2]https://almascience.eso.org/proposing/technical-handbook

[3]Following T. Bakx & J. Conway (2024), our observations are conducted using the Local Oscillator (E. Bryerton et al. 2013) and the following receivers: The Band 3 (S. Claude et al. 2008; A. R. Kerr et al. 2014), Band 4 (S. Asayama et al. 2014), Band 5 (V. Belitsky et al. 2018), Band 6 (G. A. Ediss et al. 2004; A. R. Kerr et al. 2004, 2014), Band 7 (S. Mahieu et al. 2012), Band 8 (Y. Sekimoto et al. 2008), and Band 9 (A. M. Baryshev et al. 2015).

Downloaded from https://academic.oup.com/mnras/article/544/2/1502/8318242 by guest on 21 November 2025

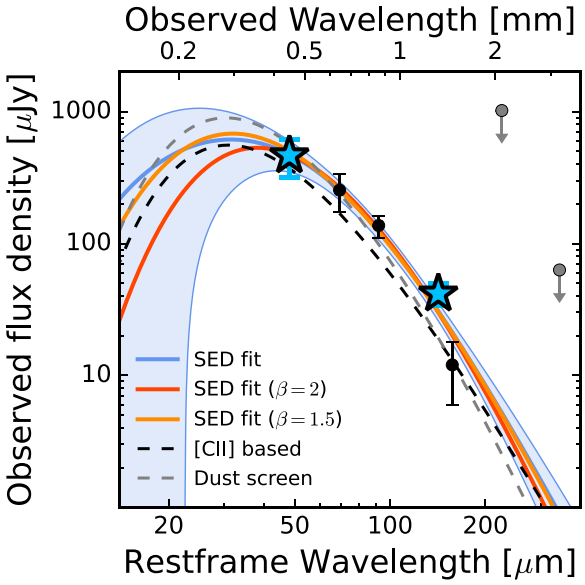

Figure 2. Three modified blackbodies are fitted to the data of Y1 (*blue stars* for novel data, and *black circles* for archival data, with upper limits in *grey circles*), with different considerations of the β_d slope. The *blue line and fill* indicates the best-fitting results of a free β_d fit, while the *red* and *orange thicker* lines indicate fits with fixed β_d of 2 and 1.5, respectively. The best-fitting temperatures (listed in Table 1) range between 72 and 94 K. The *dashed lines* show the new [C II]-based dust temperature using the methodology of L. Sommovigo et al. (2021) in *black* (see Appendix for details) and the dust scaling relation from Y. Fudamoto, A. K. Inoue & Y. Sugahara (2023) in *grey*.

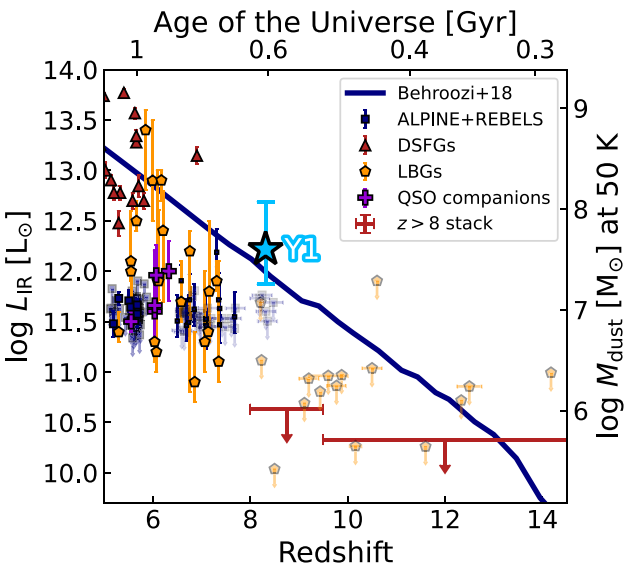

Figure 3. The infrared luminosity as a function of redshift of Y1 (*light blue star*) is compared against those of individual and stacked $z > 8$ sources that remain undetected in deep sub-mm observations (*dark red triangles*; Bakx et al. in prep.), as well as similar Lyman-break galaxies at $z = 5 - 15$ (*orange pentagons*; N. Laporte et al. 2019; A. L. Faisst et al. 2020; Y. Harikane et al. 2020; Y. Sugahara et al. 2022; I. Mitsuhashi et al. 2024b and Bakx et al. in prep.), UV-detected galaxies targeted in the ALMA Large Programmes ALPINE and REBELS (*blue*, with upper limits in *light blue squares*; M. Béthermin et al. 2020; O. Le Fèvre et al. 2020; R. J. Bouwens et al. 2022; H. Inami et al. 2022), quasar-companion galaxies (*purple pluses*; B. P. Venemans et al. 2020; T. J. L. C. Bakx et al. 2024), and dusty star-forming galaxies (*red triangles*; C. Reuter et al. 2020; G. J. Bendo et al. 2023; D. Ismail et al. 2023). A model predicting the brightest dusty galaxy from a 0.2 square degree survey size, assuming $T_d = 50$ K and a dust-to-stellar mass ratio of 0.01 (*blue line*; P. Behroozi & J. Silk 2018). Note that the warm dust temperature of Y1 causes its high luminosity with a more modest dust mass of $\sim 1.4 \times 10^6\,M_\odot$.

dust temperature of 91^{+62}_{-35} K and a β_d of $1.52^{+1.09}_{-0.75}$. Most importantly, the demagnified infrared luminosity of Y1 is $1.0^{+1.8}_{-0.6} \times 10^{12}$ $L_\odot$, indicative of an Ultra-Luminous Infrared Galaxy (ULIRG) at redshift 8.31. We explore the alternative to using a 12 ± 6 μJy data point for the Band 5 flux density based on UVMULTIFIT (I. Martí-Vidal et al. 2014) analysis, finding that the results do not change when taking a 3σ upper limit based on the χ^2 error propagation as detailed in M. Sawicki (2012). Using this χ^2 error propagation, the exclusion of the two upper limits in Bands 3 and 4 do not significantly change the fitting results.

We note that the spectrum appears well represented by a single modified blackbody, whereas before the availability of the Band 9 data, convergence of the fit was not possible with flat priors (T. J. L. C. Bakx et al. 2020b; H. S. B. Algera et al. 2024a). The only stand-out data point is from the Band 6 data, which has a much larger beam size compared to all other frequencies. Although little additional flux is seen in our curve-of-growth analysis on the other bands, this larger beam could include more extended dust missed by other observations, biasing the dust temperature and far-infrared luminosity to slightly lower values. Smoothing all data to the same resolution as Band 6 results in significantly larger uncertainties on the flux measurement, and cannot constrain the dust temperature measurement through a modified blackbody fit. Excluding the Band 6 data provides a similar dust temperature (88^{+63}_{-31} K), a steeper β_d ($= 1.88^{+1.04}_{-0.84}$) and increases the infrared luminosity by roughly $\sim$ 10 per cent, which falls within the current best-fitting uncertainty. Alternatively, if the Band 5 data is biased low, the resulting dust temperature fit excluding the Band 5 data results in much higher dust temperatures (116^{+46}_{-52} K) and substantially lower β_d ($= 0.8^{+0.9}_{-0.5}$), as well as a 10 per cent higher infrared luminosity.

If we take a fiducial $\beta_d = 2.0$ or 1.5, we find a more accurate dust temperatures of 72^{+10}_{-9} and 94^{+17}_{-14} K, respectively. However there is no appreciable improvement of the error of dust mass ($1.9^{+0.7}_{-0.5}$ and $1.4^{+0.5}_{-0.4} \times 10^6\,M_\odot$, resp.) nor luminosity, while finding ULIRG or ULIRG-like luminosities. We note that the assumption on a single dust temperature is a likely oversimplification (L. Dunne & S. A. Eales 2001; C. Behrens et al. 2018; L. Liang et al. 2019; F. Di Mascia et al. 2021). Simulation-based analytical models with an assumed lognormal distribution in dust temperatures predict that relatively wide distributions are necessary to strongly affect the total dust mass and infrared luminosity estimates (L. Sommovigo & H. Algera 2025). Similar to the $z = 7.1$ galaxy A1689-zD1, the accuracy of these latter parameters thus depends solely on observational uncertainties, indicating that we fully trace the dust emission in this source.

4 IMPLICATIONS

4.1 A ULIRG at redshift 8

Y1 is a rest-frame UV-selected galaxy identified in a cluster-lensed field. While its initial identification was through bright UV-emission ($M_{UV} = -20.9$), its modest dust mass obscures a large portion of the star formation, which in turn heats it up to warm temperatures. Fig. 3 shows the associated infrared luminosity of Y1, indicating its position as the one of the infrared-brightest objects in the $z > 7$

Downloaded from https://academic.oup.com/mnras/article/544/2/1502/8318242 by guest on 21 November 2025

Universe, and only galaxy with a direct dust detection above $z > 8$ to date. Below, we will discuss Y1 in the context of dust in the high-redshift galaxy population.

ALMA has observed roughly ten sources beyond $z > 8.3$, but has not yet identified dust emission (a compilation and stack is provided in Bakx et al. in prep.). As such, Y1 represents the vanguard of dust in the Universe, and its high temperature immediately provides it a non-negligible luminosity. Lyman-break galaxies at $z = 5 - 8$ have been detected in their dust continuum (N. Laporte et al. 2019; A. L. Faisst et al. 2020; Y. Harikane et al. 2020; Y. Sugahara et al. 2022; I. Mitsuhashi et al. 2024b), through for example the stunning discovery of dust at $z = 7.13$ in A1689-zD1 (D. Watson et al. 2015; K. K. Knudsen et al. 2017; T. J. L. C. Bakx et al. 2021; H. B. Akins et al. 2022). Since 2017, ALMA large programmes have aimed to characterize the dust emission of UV-detected galaxies, with success rate between 30 and 50 per cent (M. Béthermin et al. 2020; O. Le Fèvre et al. 2020; R. J. Bouwens et al. 2022; H. Inami et al. 2022; H. S. B. Algera et al. 2023). It is important to realize that these surveys primarily search for dust surrounding the [C II] 158 μm line, and consequently, this characterization would identify Y1 as a dust-poor system.[4] The UV-identified objects studied by the REBELS large programme (R. J. Bouwens et al. 2022) appear to have more massive dust reservoirs, and perhaps as a consequence of this, much lower dust temperatures (A. Ferrara et al. 2022; L. Sommovigo et al. 2022a; H. S. B. Algera et al. 2024a).

At redshifts below 7, galaxies can be identified through their dust emission directly. Infrared surveys, starting with the mapping of the *Hubble* Deep Field in 1997 (I. Smail, R. J. Ivison & A. W. Blain 1997; D. H. Hughes et al. 1998), in the sub-mm (e.g. *Herschel Space Observatory* and James Clerk Maxwell Telescope/Submillimetre Common-User Bolometer Array-2) and mm (e.g. *Planck*, South Pole Telescope, Atacama Cosmology Telescope) have identified over a million objects across fields with tens of square degrees to the entire sky. Consequently, these surveys readily detect dusty star-forming galaxies (DSFGs) with (apparent) luminosities beyond $> 10^{12.5}\,L_\odot$ (S. Berta et al. 2010, 2011; C. Gruppioni et al. 2013). The dust temperatures of these objects are low ($\sim 30 - 40$ K, albeit this T_d is potentially subject to optical depth effects; e.g. (C. Reuter et al. 2020; G. J. Bendo et al. 2025)), but the vast dust reservoirs ($\sim 10^{9-10}\,M_\odot$) of these systems (G. J. Bendo et al. 2023; D. Ismail et al. 2023) dominate the extragalactic infrared emission (J. A. Zavala et al. 2021).

The availability of [C II] in favourable weather bands 6 and 7 – and its important diagnostic value – have incentivized observations of $z = 5 - 7.5$ quasars from large-area surveys. The combined survey area within the fields of view of these observations have resulted in tens of quasar-companion galaxies (QCGs) detected through line and/or continuum emission, which provided an important third probe between the UV- and sub-mm selection of galaxies in the early Universe (R. Decarli et al. 2017; B. P. Venemans et al. 2020; T. J. L. C. Bakx et al. 2024; I. F. Leeuwen et al. 2024). Similar to previous interferometric blank field observations (the ALMA Lensing Cluster Survey and the ALMA Spectroscopic Survey in the *Hubble* Ultra Deep Field), these aim to detect a large number of distant objects through their [C II] emission. Interestingly, these galaxies appear to have low-dust temperatures ($\lesssim 30$ K), large dust masses ($\sim 10^8\,M_\odot$, T. J. L. C. Bakx et al. 2024), and high-UV dust obscuration ($\gtrsim 93$ per cent; I. F. Leeuwen et al. 2024), making them hard to include as a galaxy population from UV and even finding them directly in continuum-selected sub-mm observations.

Y1 has a relatively low dust-to-stellar mass ratio of $1.4^{+1.3}_{-0.5} \times 10^{-3}$, in line with expected yields from supernovas and asymptotic giant branch (AGB) stars (R. Schneider & R. Maiolino 2024). The most massive of these stars, with $\sim 8\,M_\odot$, require at least 30–100 Myr to reach their AGB phase (E. Dwek & I. Cherchneff 2011; M. Lugaro et al. 2012). Assuming the majority of the dust in Y1 is produced through supernovae instead, based on the methodology in M. J. Michałowski (2015), we estimate a required supernova yield of $y = 0.07^{+0.06}_{-0.03}\,M_\odot$/SN (c.f., H. S. B. Algera et al. 2024b, for an extended discussion). This is in line with models for supernova dust production (~ 0.2–$1\,M_\odot$; M. Matsuura et al. 2011; R. Indebetouw et al. 2014; I. De Looze et al. 2017; M. Niculescu-Duvaz et al. 2022), as well as the expected destruction through reverse shocks that can destroy potentially up to 90 per cent of the dust formed (S. Bianchi & R. Schneider 2007; F. Kirchschlager et al. 2019, 2024). Since the effect of dust destruction in Y1 (and elsewhere) are uncertain, it is reassuring to see the predicted dust yields below the theoretical estimates.

Although the dust-to-stellar mass ratio is relatively low, an analytical one-dimensional dust evolution study predicts that this ratio still requires some time to achieve sufficient dust production from dust production sources (D. Toyouchi et al. 2025). Even in environments with enhanced destruction, fluid-dynamical models of dust production suggest that these dust-to-stellar mass ratios are not uncommon (C. J. Esmerian & N. Y. Gnedin 2024). *Hubble* imaging revealed a young (~ 4 Myr) stellar population. Due to the young age of this stellar population, models predict it is unable to produce the observed dust and oxygen emission in ALMA imaging. This implied the existence of a pre-existing massive, older stellar component (Y. Tamura et al. 2019), based on the dust production model from R. S. Asano et al. (2013). Updated spectral modelling of *JWST* imaging find similarly-young stellar populations (Z. Ma et al. 2024; c.f. A. Harshan et al. 2024), which suggests that a pre-existing stellar population is responsible for the dust in Y1. If Y1 would be a progenitor of the most massive REBELS galaxies and QCGs, which have roughly an order of magnitude more massive stellar populations (H. S. B. Algera et al. 2023), there is a need for a substantial increase in the efficiency of dust production in its subsequent 200 Myr, potentially due to the onset of rapid ISM dust growth (H. Algera et al. 2025).

A comparison to the galaxy evolution model of P. Behroozi & J. Silk (2018) provides a measure of the maximum infrared luminosity for a galaxy detected in a field observed by deep optical observations, expected to hold true for most LBGs, ALPINE, REBELS, and the $z > 8$ LBGs, but not for DSFGs and QCGs identified from much larger area surveys. This comparison assumes a total survey size of 0.2 deg^2 roughly similar to the deep fields from *Hubble* surveys (P. A. Oesch et al. 2016). The highest stellar masses achieved in the model of P. Behroozi & J. Silk (2018) are subsequently converted to an expected infrared luminosity (assuming $\beta_d = 2$ and $T_d = 50$ K) through a high stellar-to-dust mass ratio of 0.01. Y1 is in line with the highest expected infrared luminosity at this redshift, but primarily because of its high dust temperature, while its modest stellar mass instead lies well within the range expected for distant galaxies.

[4] Although the galaxy nearest to Y1 in redshift with infrared emission, A2744-YD4, has a similar indication of warm dust (N. Laporte et al. 2017; C. Behrens et al. 2018; N. Laporte et al. 2019; H. S. B. Algera et al. 2024a), its nature turned out to be more complicated (T. Hashimoto et al. 2023; T. Morishita et al. 2023). Thus, dust temperatures need to be carefully re-evaluated with higher-resolution ALMA observations

Downloaded from https://academic.oup.com/mnras/article/544/2/1502/8318242 by guest on 21 November 2025

4.2 Warm dust in the Epoch of Reionization

Ever since the non-detection of dust continuum around the [C II] emission of Y1, the suspicion of a warm dust reservoir in Y1 has existed. The observations reported in this paper now confirm the warm nature of the dust through an accurate census of the dust close to the peak of the dust continuum.

Given the importance of warm dust in the early Universe, studies have reported both the direct fitting of the observed data and the implementation of dust models to limit the uncertainty on the dust temperature. The first fit of the dust temperature (T. J. L. C. Bakx et al. 2020b) provided a χ^2-based lower limit on the dust temperature of > 80 K. Using a more extensive fitting routine, H. S. B. Algera et al. (2024a) reports on a lower limit at 3σ of > 88 K. We choose to take an optically thin dust profile, as the estimated opacity at the observed wavelengths is negligible, assuming a dust mass limit of $\sim 1 \times 10^6$ M$_\odot$. Theoretical models of this source report similarly warm dust temperatures, with the scaling relation modelling by L. Sommovigo et al. (2021) reporting a dust temperature of 82^{+16}_{-19} K. Using the 91 μm flux from Y. Tamura et al. (2023), a re-run of the modelling by L. Sommovigo et al. (2021) on Y1 finds similar results of 94^{+8}_{-11} K (see Appendix Fig. B1). Geometric arguments using radiative transfer under a clumpy sphere geometry in A. K. Inoue et al. (2020) and Y. Fudamoto et al. (2023) predict a dust temperature of 95^{+13}_{-16} K. These studies predict an associated demagnified infrared (8 to 1000 μm) luminosity of $\gtrsim 10^{12}$ L$_\odot$, in line with a local ULIRG.

Fig. 4 shows the dust temperature of Y1 from a direct dust temperature fit from a modified blackbody against those of the [C II]-based dust temperature estimate from L. Sommovigo et al. (2021) and the clumpy dust geometry estimate from A. K. Inoue et al. (2020) and Y. Fudamoto et al. (2023). These are compared against $z < 4$ galaxy fits (C. Schreiber et al. 2018) and a stack (M. Béthermin et al. 2015). At $z > 4$, the dust temperatures come mostly from Lyman-break galaxies (A. L. Faisst et al. 2020; Y. Harikane et al. 2020; Y. Sugahara et al. 2022; J. Witstok et al. 2023a; H. S. B. Algera et al. 2024a, b), as well as stacks of ALPINE data (M. Béthermin et al. 2020). Two dust temperature scaling relations are shown, with one relation based on an empirical extrapolation of the $z < 4$ data (C. Schreiber et al. 2018). The other scaling relation is based on a physical model of dust attenuation in low metallicity and high-optical-depth regions (L. Sommovigo et al. 2022a).

The dust temperature measures using the additional information, including [C II] and the dust geometry, appear to provide a reasonable estimate, in line with the improved SED fit. Prior to the Band 9 data, only a lower limit at 80 K was available (T. J. L. C. Bakx et al. 2020b; H. S. B. Algera et al. 2024a). The short-wavelength observation now confirms the high-dust temperature implied by the non-detection at 160 μm rest-frame, and places Y1 as one of the galaxies with the highest dust temperatures in the observed Universe, assuming an optically thin modified blackbody. This high-dust temperature is in line with the behaviour of low-metallicity galaxies seen in the scaling relation in L. Sommovigo et al. (2022a). The metallicity measurements of Y1 find a $\sim 0.1 - 0.2$ Z$_\odot$ system (Y. Tamura et al. 2019; A. Harshan et al. 2024), with modest variation in metallicity across the source (Z. Ma et al. 2024, c.f.), in line with the observed high-dust temperature of ~ 90 K. In these low-metallicity environments, dust is unable to self-shield, allowing for much higher dust temperatures than in more dust- and metal-rich galaxies, such as the higher metallicity REBELS galaxies (H. S. B. Algera et al. 2024a, b; L. E. Rowland et al. 2025).

As a consequence of the high-dust temperature, the infrared luminosity is ~ 35 times higher than the typically assumed 50 K

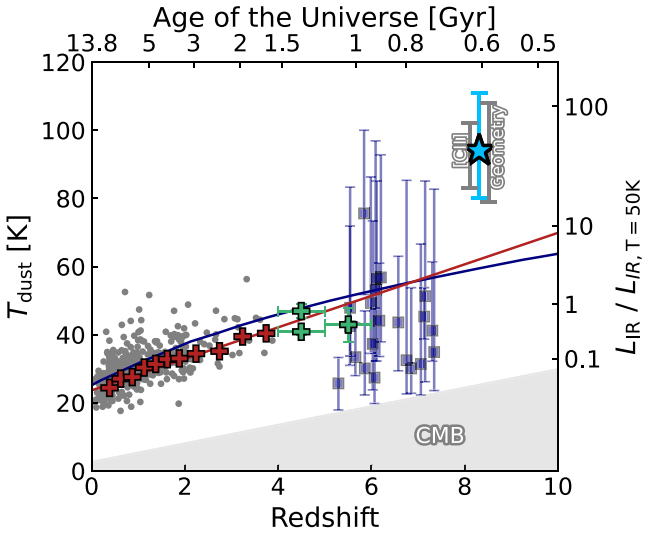

Figure 4. Dust temperature of galaxies and samples as a function of redshift. The dust temperature estimate for Y1 is shown in *light blue*, and is compared to previous estimates based on [C II] (L. Sommovigo et al. 2021) and on a clumpy dust distribution geometric estimate (Y. Fudamoto et al. 2023) in grey. Dust temperatures obtained for lower-redshift sources at $z < 4$ are shown in grey points (C. Schreiber et al. 2018), and for higher-redshift galaxies in blue squares (A. L. Faisst et al. 2020; Y. Harikane et al. 2020; Y. Sugahara et al. 2022; J. Witstok et al. 2023a; H. S. B. Algera et al. 2024a, b). Dust temperature evolution based on stacked SEDs is shown in *red and green pluses*, which are shown to increase linearly with redshift up to $z = 6$ (M. Béthermin et al. 2015; C. Schreiber et al. 2018; M. Béthermin et al. 2020). The best-fit from C. Schreiber et al. (2018) is shown in a *red line*, while the average physically motivated dust temperature relation from L. Sommovigo et al. (2022a) is shown in a *blue line*. Prior to the Band 9 data, only lower limits were available on Y1. The other axis indicates the change in infrared luminosity compared to 50 K, indicating the strong dependence of infrared luminosity on dust temperature, and the greyed-out region indicates the CMB temperature at a given redshift.

luminosity on a single continuum data point (e.g. R. Bouwens et al. 2020). The unobscured star-formation rate of Y1 is 14 ± 1 M$_\odot$ yr^{-1} for a system with a total UV luminosity of $(4.00 \pm 0.18) \times 10^{10}$ L$_\odot$ (T. Hashimoto et al. 2019; Z. Ma et al. 2024). Meanwhile, assuming an IR luminosity-to-SFR (Star Formation Rate) conversion factor of 1.73×10^{-10} M$_\odot$ yr^{-1}/L$_\odot$ (valid for a Salpeter $1 - 100$ M$_\odot$ Initial Mass Function), the obscured star-formation rate of Y1 is 173 M$_\odot$ yr^{-1}. Consequently, the obscured fraction of star-formation of Y1 is high, at 93 ± 5 per cent. Fig. 5 shows the high obscured fraction of Y1 against the average obscuration fractions of galaxies (Y. Fudamoto et al. 2020b; H. S. B. Algera et al. 2023; R. A. A. Bowler et al. 2024; I. Mitsuhashi et al. 2024a, b) and scaling relations (K. E. Whitaker et al. 2017; Y. Fudamoto et al. 2020b) at lower redshifts. Y1 lies above these relations, indicating it has a high obscured fraction of star-formation when compared to samples of galaxies at lower redshift.

The high luminosity of Y1 originates from an infrared-dominated spectrum, and places it in the ULIRG (or ULIRG-like) regime. At cosmic noon, ULIRGs are typically found to be dust-obscured galaxies with cold dust (e.g. G. J. Bendo et al. 2023, 2025) and high dust-to-gas ratios (e.g. M. Hagimoto et al. 2023). Alternative to these colder galaxies, dust temperatures of about 90 K are observed in other high-z sources and in some cases associated to AGN host galaxies. For example, Wide-field Infrared Survey Explorer (WISE) identified a set of hot-dust obscured galaxies (affably coined HotDOGs; C.-W.

Downloaded from https://academic.oup.com/mnras/article/544/2/1502/8318242 by guest on 21 November 2025

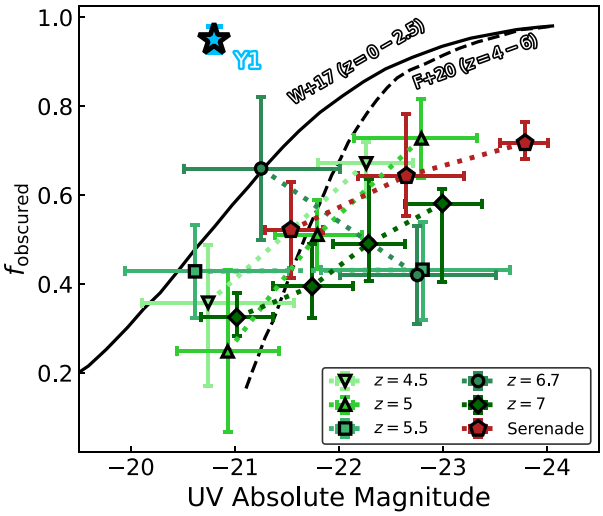

Figure 5. Obscured fraction of the star formation against the observed absolute UV magnitude ($M_{\rm UV}$–$f_{\rm obs}$). Y1 lies above the relation at a lower absolute UV-magnitude than previous stacked results. The increasing hues of *green downward triangles, triangles, squares, circles, diamonds*, and *pentagons* are the results at $z \sim 4.5$, 5, 5.5, 6.7, and 7 (Y. Fudamoto et al. 2020b; H. S. B. Algera et al. 2023; R. A. A. Bowler et al. 2024; I. Mitsuhashi et al. 2024a, b), respectively. The scaling relations from K. E. Whitaker et al. (2017) and Y. Fudamoto et al. (2020b) are shown in solid and dashed lines, respectively.

Tsai et al. 2015), where the bolometric luminosity is dominated by a hot dust component likely powered by massive Active Galactic Nuclei (AGN; R. Fernández Aranda et al. 2025). Submm bright hot-DOG host galaxies have been found harbour sub-millimetre galaxy-like starbursts with temperatures of $60 - 100$ K (e.g. L. Fan et al. 2016). While the optical emission lines indicate a potential narrow-line AGN in Y1, the presence of two dust emission peaks in the high-resolution Band 7 data (Y. Tamura et al. 2023) implies that there is not a single central heating source of the dust. Both of these components are likely originating from separate warm dust components, as otherwise one of the two faint components would be detected in the Band 5 data (see Astles et al. in prep.). The presence of multiple warm dust components could in part be due to heating by this narrow-line AGN (e.g. T. Tsukui et al. 2023; R. Fernández Aranda et al. 2025), but is more likely to originate from stellar emission, in line with models of compact, young star-forming regions enshrouded in molecular clouds (C. Behrens et al. 2018; A. Pallottini et al. 2022).

A discrepancy between the obscured and unobscured cosmic star-formation rate density has become apparent in the early Universe (e.g. C. M. Casey et al. 2018). Recent works using deep sub-mm (ALMA) and radio (Very Large Array) (e.g. M. Novak et al. 2017; C. Gruppioni et al. 2020; M. Talia et al. 2021) indicate a high SFRD with little evolution out to redshifts beyond $z > 3$. The uncertainty in the obscured SFRD at high redshift is due to the lack of deep sub-mm surveys capable of characterizing the dust temperature at high-z. The purported hot dust temperature expected for low-metallicity systems (L. Sommovigo et al. 2022a) could produce a population of low-metallicity ($< 0.2\,Z_\odot$) young galaxies with small but excessively hot dust bodies that dominate the cosmic SFRD. Missed in longer-wavelength surveys (J. A. Zavala et al. 2021; A. S. Long et al. 2024), the high-obscuration fraction of Y1-like galaxies (93 ± 6 per cent) would be enough to flatten the < 1 dex drop in cosmic SFRD between $z = 3$ to 8. Meanwhile, the warm dusty phase is likely very short. The high-specific star-formation rate of $187\,{\rm Gyr}^{-1}$ indicates the likely short-lived nature of these systems, which is in line with young star-bursting systems.

Similarly, the contrast between the [C II] and [O III] emission implies an ionized gas region outflowing from Y1 with $\sim 100\,{\rm km\,s}^{-1}$. This outflowing cloud (about one-third of all [O III] luminosity) traces the UV-emission (Bakx et al. in prep.). As the star-formation rate is $> 150\,{\rm M}_\odot\,{\rm yr}^{-1}$ within this ~ 1 kpc^2 system, and the small *JWST*-estimated stellar mass ($\sim 10^9\,{\rm M}_\odot$) is unlikely to keep this gas contained (B. H. Andrews & T. A. Thompson 2011; c.f., M. Kohandel, A. Pallottini & A. Ferrara 2025).

Such episodic star formation in the early Universe can drive fast metal-rich winds into the circumgalactic medium. Indications of star-formation driven winds are fundamental ingredients of hydrodynamical (e.g. S. Arata et al. 2019), semi-analytical (e.g. L. Y. A. Yung et al. 2019), and analytical (A. Ferrara et al. 2023) models, as well as crucial for explaining dust (T. J. L. C. Bakx et al. 2024), the scatter in the mass–metallicity relation (A. Pallottini et al. 2025), and emission line observations (S. Carniani et al. 2024) in low-mass galaxies in the early Universe. The $\sim 100\,{\rm km\,s}^{-1}$ velocity offset seen through combined [C II] and [O III] emission is in line with the analytically predicted velocities of radiation-driven winds (A. Ferrara et al. 2023; A. Ferrara 2024).

4.3 IRX-$\beta_{\rm UV}$ relation in the early Universe

Dust obscures our UV and optical view of star formation by preferentially obscuring the blue components of the stellar emission. The subsequent heating of the dust results in bright (sub)mm emission from galaxies. The dust obscuration can be quantified both through the difference between obscured and unobscured emission, as well as through the reddening of the rest-frame UV emission. Common dust-attenuation curves can be used to estimate the sub-mm emission and associated dust-obscured star-formation rate directly from the UV luminosity ($L_{\rm UV}$) and slopes ($\beta_{\rm UV}$) that identify $z > 7$ galaxies through the so-called InfraRed eXcess (IRX $= \log_{10} L_{\rm IR}/L_{\rm UV}$). This correlation between $\beta_{\rm UV}$ and IRX balances the absorbed UV emission that is subsequently re-emitted in the sub-mm regime. However, a correlation between IRX and $\beta_{\rm UV}$ can only occur if the UV and dust-emitting regions are cospatial (J. H. Howell et al. 2010; A. L. Faisst et al. 2017), as otherwise the UV emission can be dominated by bright unobscured stars that outshine the contribution of the obscured stars which heat the dust, further exacerbated by complex geometries (A. P. Vijayan et al. 2024). Stark deviations from this IRX-$\beta_{\rm UV}$ relation are evidenced by the existence of optically dark galaxies (e.g. C. M. Casey et al. 2019; T. Wang et al. 2019; Y. Fudamoto et al. 2021; J. A. Zavala et al. 2021) and optically detected galaxies (e.g. S. Carniani et al. 2017; R. A. A. Bowler et al. 2022, 2024; H. Inami et al. 2022) with significant spatial offset between their ALMA and *Hubble Space Telescope (HST)* data, as well as the identification of dusty star-forming galaxies before them (I. Smail et al. 1997; D. H. Hughes et al. 1998). Observations in the UV can thus not make up for direct infrared observations, as also supported by theoretical studies and simulations (e.g. A. Ferrara et al. 2022).

The combined observations at ~ 0.1 arcsec resolution from *JWST* and ALMA Band 7 allow us to compare this reddening to the total emitted (sub)mm emission. Fig. 6 shows the resolved $\beta_{\rm UV}$ map from *JWST* at ~ 200 pc resolution. We use the filters F150W, F200W, and F277W to produce the resolved $\beta_{\rm UV}$ map, which are reprojected and smoothed to the same common point-spread function (PSF), using the empirically derived PSFs for the *JWST* filters. The observed wave-

Downloaded from https://academic.oup.com/mnras/article/544/2/1502/8318242 by guest on 21 November 2025

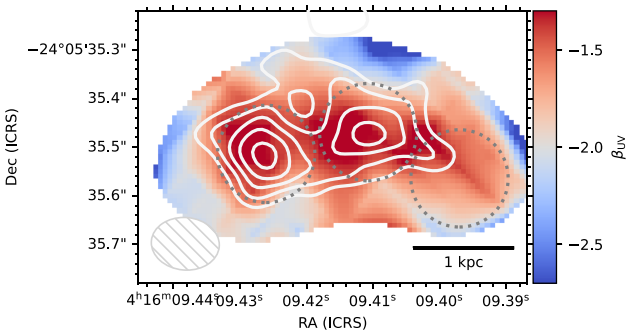

Figure 6. The spatially resolved UV-continuum slope ($\beta_{\rm UV}$) relative to the Band 7 dust continuum (*white contours*). The peak positions of the ALMA-based dust continuum is cospatial to relatively high, red values of $\beta_{\rm UV}$. This shows that the dust obscuration of stellar emission in both sub-mm and optical colours originate from similar regions. The small circles indicate the regions where the IRX-$\beta_{\rm UV}$ is evaluated in a resolved fashion in Fig. 7.

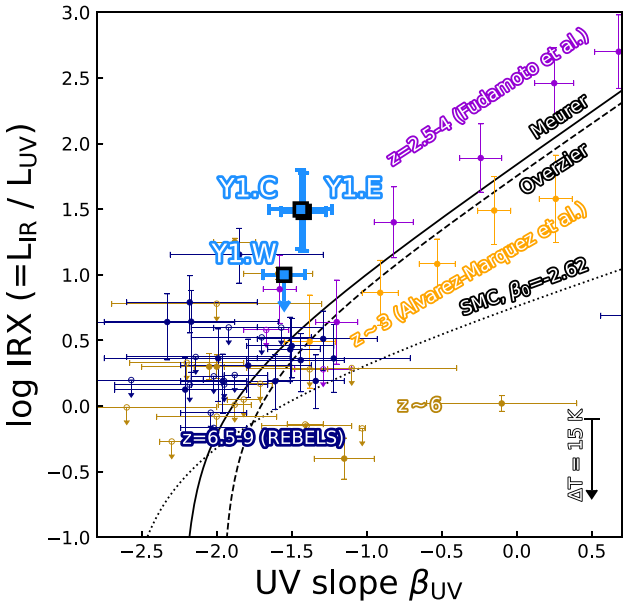

Figure 7. The infrared excess of Y1 is evaluated at three locations and compared against the observed UV continuum slope ($\beta_{\rm UV}$). These are compared to previous measurements of the galaxies at $z = 2.5$–4 (Y. Fudamoto et al. 2020a, purple), $z \sim 3$ (J. Álvarez-Márquez et al. 2019, orange), $z \sim 4.5$ and $z \sim 5.5$ (Y. Fudamoto et al. 2020b, blue circles), and $z \sim 6$ (R. A. A. Bowler et al. 2024, golden circles). These are further compared against the best-fitting relations from local (M. L. Prevot et al. 1984; G. R. Meurer, T. M. Heckman & D. Calzetti 1999; D. Calzetti et al. 2000; K. D. Gordon et al. 2003; R. A. Overzier et al. 2011; T. T. Takeuchi et al. 2012) and high-z galaxies (e.g. J. Álvarez-Márquez et al. 2016; N. A. Reddy et al. 2018; Y. Fudamoto et al. 2020b). A spatial variation in dust temperature of 15 K is indicated by an arrow in the bottom-right of the panel.

lengths are 15 010 Å for the F150W, 19 880 Å for the F200W and 27 760 Å for the F277W filter. These images are astrometrically verified against *Gaia* stars and previous *Hubble* imaging (Y. Tamura et al. 2019), and are shown in Appendix Fig. C1. A combined RGB-image of the smoothed *JWST* imaging can be found in Appendix Fig. C2. Per pixel, a single $\beta_{\rm UV}$ is fit to the fluxes and error maps across three wavelengths, overcoming the uncertainties found to occur in previous measurements from colour–colour slopes (F. Cullen et al. 2024).

In an effort to exclude line confusion, we explore the available NIRSpec Integral Field Unit (*JWST* PID 1208; P.I. Chris Willott) and NIRSpec Multi-Object Spectroscopy (A. Harshan et al. 2024). While the stellar continuum is visible in the Integral Field Unit and PRISM spectroscopy, no bright line emission is visible nor expected in within the expected photometric filters *F150W*, *F200W*, and *F277W*. Consequently, we predict the effect of line contamination to the $\beta_{\rm UV}$ image to be negligible. Although beyond the scope of this paper, we note that future work could continue this investigation into the resolved attenuation through direct measurement of the Balmer line attenuation, which is less affected by stellar age and the assumption on the intrinsic $\beta_{\rm UV,0}$ slope to calculate the A_V.

The two dust continuum peaks are close to the peaks in the reddest part of the $\beta_{\rm UV}$ map, indicating that the dust emission appears cospatial with $\beta_{\rm UV} = -1.2$ to -1.7 (Y. Tamura et al. 2019; A. Harshan et al. 2024). Meanwhile, the spur-like feature to the south–west part of Y1 is cospatial to a red component with $\beta_{\rm UV} \approx -1.6$, which is brightly seen through UV imaging but not in dust continuum imaging of Y1.

Fig. 7 quantifies the UV-continuum slope and the infrared-to-UV emission through the so-called IRX-β relation. The $\beta_{\rm UV}$ is extracted at the peak dust emission, as well as at the Western component that does not show indications of dust emission in 0.2 arcsec apertures. The resolved infrared and UV luminosity are derived by their respective contribution to the total flux in ALMA Band 7 and F200W NIRCam imaging.

The two dust-emitting regions lie above the observed scaling relations, in line with the *dust screen with holes* scenario (G. Popping, A. Puglisi & C. A. Norman 2017). CLOUDY modelling of this galaxy (M. Hagimoto et al. 2025), including its spectral lines and dust emission, predicts a low covering fraction of neutral gas in this galaxy of 25 per cent, suggesting 75 per cent of the ionized gas region is exposed to intercloud space. This is similar to dwarf galaxies seen in the local Universe (D. Cormier et al. 2019). Indeed, while the dust and $\beta_{\rm UV}$ values imply that dust absorption coincide, the deviation from the IRX-$\beta_{\rm UV}$ indicates that the dust attenuation of stars occurs on scales smaller than those probed by *JWST* and ALMA at $\sim$ 200 pc (J. M. D. Kruijssen & S. N. Longmore 2014; J. M. D. Kruijssen et al. 2019; F. Di Mascia et al. 2025). Potentially, temperature variation across Y1 can affect the resolved IRX measure. The dust temperature in both components is likely still high, as otherwise it would be detected in the resolved 160 μm dust emission map (see Bakx et al. in prep.). Fig. 7 indicates the effect of a large dust-temperature variation of $\sim$ 15 K (H. B. Akins et al. 2022; R. A. A. Bowler et al. 2022; T. Tsukui et al. 2023; R. Fernández Aranda et al. 2025). In this extreme case, this could reduce the IRX-$\beta_{\rm UV}$ discrepancy of one of the components of Y1, while exacerbating the discrepancy for the other. A more detailed analysis of the spatial variation of dust temperature is beyond the scope of this work.

This measure can be further quantified through the so-called molecular index, defined as $I_{\rm m} = (F_{158}/F_{1500})/(\beta_{\rm UV} + 2.6)$ (A. Ferrara et al. 2022), that compares the fluxes F at the sub-mm (158 μm) against those in the rest-frame optical (1500 Å), and compares this against the steepness of the UV continuum slope. For Y1, the observed F_{1500} flux across the source is 0.124 ± 0.03 μJy (Z. Ma et al. 2024) based on the nearest *JWST* filter F150W, with the $F_{158} = 12 \pm 6$ μJy. The resulting $I_{\rm m}$ ranges from 70 to 110, taking the spread in values for $\beta_{\rm UV} = -1.2$ to -1.7 seen across the source. Not exceeding the threshold for strongly segregated obscured and unobscured regions of $I_{\rm m} > 1120$, the ISM is likely a mixture of mixed and separated (A. Ferrara et al. 2022; L. Sommovigo et al. 2022b). This is in line with the previous finding that the bulk emission of stars and dust emission is unassociated on the scales of $\sim$ 500 pc

Downloaded from https://academic.oup.com/mnras/article/544/2/1502/8318242 by guest on 21 November 2025

(Y. Tamura et al. 2023), as well as its low-neutral gas covering fraction of ~ 25 per cent (M. Hagimoto et al. 2025). In this scenario, strong stellar feedback from young stellar populations exposes them to low-attenuation sightlines, where they outshine the redder, attenuated emission from obscured stellar regions (S. Arata et al. 2019).

5 CONCLUSIONS

The Band 9 observations reported in this paper confirm that Y1 is a ULIRG at redshift 8.3 by tracing its mm and sub-mm dust spectrum. Although this source was initially detected with a similar sub-mm emission as $z = 7 - 8$ galaxies (Y. Tamura et al. 2019), its uniquely high-dust temperature (91^{+62}_{-35} K) results in a ULIRG-like infrared luminosity, with a high-obscured fraction of star formation (~ 93 per cent). The short-wavelength observations thus confirm the initial suspicions of a high-dust temperature, raised by the non-detection of the Band 5 emission (T. J. L. C. Bakx et al. 2020b). The furthest direct detection of dust emission to-date thus originates from a standout system with a high temperature, luminosity, and obscuration, with only a modest dust mass in line with typical models of supernova and AGB dust production. When spatially comparing the resolved Band 7 dust emission to the dust-attenuated UV continuum slope ($\beta_{\rm UV}$), the dust-emitting regions lie cospatial to optically obscured regions. However, the elevated position of Y1 in the IRX-$\beta_{\rm UV}$ plot indicates the existence of obscured stellar components that are missed by the UV observations of this ULIRG. This suggests that dust is only partially covering the UV-emitting regions, and/or that dust and UV-emitting regions are dissociated on scales smaller than 200 pc, i.e. those probed by *HST*, *JWST*, and ALMA.

ACKNOWLEDGEMENTS

The authors kindly thank the anonymous referee for their insightful comments and suggestions to improve this manuscript. This paper makes use of the following ALMA data: ADS/JAO.ALMA 2013.1.00999.S, 2017.1.00225.S, 2019.1.00343.S, 2019.1.01350.S, 2021.1.00075.S, 2022.1.01356.S, 2024.1.00537.S, and 2024.1.00995.S. Financial support from the Knut and Alice Wallenberg foundation is gratefully acknowledged through grant no. KAW 2020.0081. KK acknowledges support from the Knut and Alice Wallenberg Foundation and the ERC Synergy Grant 'RECAP' (grant 101166930). This work was supported by NAOJ ALMA Scientific Research Grant Numbers 2018–09B and JSPS KAKENHI Nos. 17H06130, 22H04939, 23H000131, and 25H00671. JM and EI gratefully acknowledge financial support from ANID – MILENIO - NCN2024_112. EI also gratefully acknowledges financial support from ANID FONDECYT Regular 1221846. AF acknowledges support from the ERC Advanced Grant INTERSTELLAR H2020/740120.

DATA AVAILABILITY

The data sets generated during and/or analysed during the current study are available from the corresponding author on reasonable request. The codes used to reduce and analyse the ALMA data are publicly available.

REFERENCES

Akins H. B. et al., 2022, ApJ, 934, 64
Algera H. et al., 2025, preprint (arXiv:2501.10508)
Algera H. S. B. et al., 2023, MNRAS, 518, 6142
Algera H. S. B. et al., 2024a, MNRAS, 527, 6867
Algera H. S. B. et al., 2024b, MNRAS, 533, 3098
Álvarez-Márquez J. et al., 2016, A&A, 587, A122
Álvarez-Márquez J., Burgarella D., Buat V., Ilbert O., Pérez-González P. G., 2019, A&A, 630, A153
Andrews B. H., Thompson T. A., 2011, ApJ, 727, 97
Arata S., Yajima H., Nagamine K., Li Y., Khochfar S., 2019, MNRAS, 488, 2629
Asano R. S., Takeuchi T. T., Hirashita H., Inoue A. K., 2013, Earth Planets Space, 65, 213
Asayama S. et al., 2014, PASJ, 66, 57
Bakx T., Conway J., 2024, ALMA memo 627, p. E2
Bakx T. J. L. C., Eales S., Amvrosiadis A., 2020a, MNRAS, 493, 4276
Bakx T. J. L. C. et al., 2020b, MNRAS, 493, 4294
Bakx T. J. L. C. et al., 2021, MNRAS, 508, L58
Bakx T. J. L. C. et al., 2024, MNRAS, 532, 2270
Baryshev A. M. et al., 2015, A&A, 577, A129
Behrens C., Pallottini A., Ferrara A., Gallerani S., Vallini L., 2018, MNRAS, 477, 552
Behroozi P., Silk J., 2018, MNRAS, 477, 5382
Belitsky V. et al., 2018, A&A, 611, A98
Bendo G. J. et al., 2023, MNRAS, 522, 2995
Bendo G. J. et al., 2025, MNRAS, 540, 1560
Berta S. et al., 2010, A&A, 518, L30
Berta S. et al., 2011, A&A, 532, A49
Béthermin M. et al., 2015, A&A, 573, A113
Béthermin M. et al., 2020, A&A, 643, A2
Bianchi S., Schneider R., 2007, MNRAS, 378, 973
Bouwens R. et al., 2020, ApJ, 902, 112
Bouwens R. J. et al., 2015, ApJ, 803, 34
Bouwens R. J. et al., 2022, ApJ, 931, 160
Bowler R. A. A., Cullen F., McLure R. J., Dunlop J. S., Avison A., 2022, MNRAS, 510, 5088
Bowler R. A. A. et al., 2024, MNRAS, 527, 5808
Bryerton E., Saini K., Muehlberg J., Vaselaar D., Thacker D., 2013, in IEEE MTT-S International Microwave Symposium Digest. p. 6697622
CASA Team et al., 2022, PASP, 134, 114501
Calzetti D., Armus L., Bohlin R. C., Kinney A. L., Koornneef J., Storchi-Bergmann T., 2000, ApJ, 533, 682
Carniani S. et al., 2017, A&A, 605, A42
Carniani S. et al., 2024, A&A, 685, A99
Casey C. M. et al., 2018, ApJ, 862, 77
Casey C. M. et al., 2019, ApJ, 887, 55
Choban C. R., Kereš D., Hopkins P. F., Sandstrom K. M., Hayward C. C., Faucher-Giguère C.-A., 2022, MNRAS, 514, 4506
Choban C. R., Kereš D., Sandstrom K. M., Hopkins P. F., Hayward C. C., Faucher-Giguère C.-A., 2024, MNRAS, 529, 2356
Claude S. et al., 2008, in Duncan W. D., Holland W. S., Withington S., Zmuidzinas J., eds, Proc. SPIE Conf. Ser. Vol. 7020, Millimeter and Submillimeter Detectors and Instrumentation for Astronomy IV. SPIE, Bellingham, p. 70201B
Cormier D. et al., 2019, A&A, 626, A23
Cullen F. et al., 2024, MNRAS, 531, 997
De Looze I., Barlow M. J., Swinyard B. M., Rho J., Gomez H. L., Matsuura M., Wesson R., 2017, MNRAS, 465, 3309
Decarli R. et al., 2017, Nature, 545, 457
Demyk K. et al., 2017a, A&A, 600, A123
Demyk K. et al., 2017b, A&A, 606, A50
Di Mascia F. et al., 2021, MNRAS, 503, 2349
Di Mascia F., Pallottini A., Sommovigo L., Decataldo D., 2025, A&A, 695, A77
Draine B. T., 2003, ARA&A, 41, 241
Dunne L., Eales S. A., 2001, MNRAS, 327, 697
Dwek E., Cherchneff I., 2011, ApJ, 727, 63
Ediss G. A. et al., 2004, in Narayanan G., ed., Fifteenth International Symposium on Space Terahertz Technology. p. 181
Esmerian C. J., Gnedin N. Y., 2024, ApJ, 968, 113
Faisst A. L. et al., 2017, ApJ, 847, 21

Downloaded from https://academic.oup.com/mnras/article/544/2/1502/8318242 by guest on 21 November 2025

Faisst A. L., Fudamoto Y., Oesch P. A., Scoville N., Riechers D. A., Pavesi R., Capak P., 2020, MNRAS, 498, 4192
Fan L., Han Y., Nikutta R., Drouart G., Knudsen K. K., 2016, ApJ, 823, 107
Fernández Aranda R. et al., 2025, A&A, 695, L15
Ferrara A., 2024, A&A, 684, A207
Ferrara A., Hirashita H., Ouchi M., Fujimoto S., 2017, MNRAS, 471, 5018
Ferrara A. et al., 2022, MNRAS, 512, 58
Ferrara A., Pallottini A., Dayal P., 2023, MNRAS, 522, 3986
Ferrara A., Giavalisco M., Pentericci L., Vanzella E., Calabrò A., Llerena M., 2025, Open J. Astrophys., 8, 125
Finkelstein S. L. et al., 2015, ApJ, 810, 71
Fisher R. et al., 2025, MNRAS, 539, 109
Foreman-Mackey D., Hogg D. W., Lang D., Goodman J., 2013, PASP, 125, 306
Fudamoto Y. et al., 2020a, MNRAS, 491, 4724
Fudamoto Y. et al., 2020b, A&A, 643, A4
Fudamoto Y. et al., 2021, Nature, 597, 489
Fudamoto Y., Inoue A. K., Sugahara Y., 2023, MNRAS, 521, 2962
Fujimoto S. et al., 2024, ApJ, 964, 146
Gordon K. D., Clayton G. C., Misselt K. A., Landolt A. U., Wolff M. J., 2003, ApJ, 594, 279
Gruppioni C. et al., 2013, MNRAS, 432, 23
Gruppioni C. et al., 2020, A&A, 643, A8
Hagimoto M. et al., 2023, MNRAS, 521, 5508
Hagimoto M. et al., 2025, ApJ, 990, 29
Harikane Y. et al., 2020, ApJ, 896, 93
Harshan A. et al., 2024, ApJ, 977, L36
Hashimoto T. et al., 2019, PASJ, 71, 71
Hashimoto T. et al., 2023, ApJ, 955, L2
Hirashita H., Chen C.-C., 2023, MNRAS, 526, 4710
Howell J. H. et al., 2010, ApJ, 715, 572
Hughes D. H. et al., 1998, Nature, 394, 241
Inami H. et al., 2022, MNRAS, 515, 3126
Indebetouw R. et al., 2014, ApJ, 782, L2
Inoue A. K. et al., 2016, Science, 352, 1559
Inoue A. K., Hashimoto T., Chihara H., Koike C., 2020, MNRAS, 495, 1577
Ismail D. et al., 2023, A&A, 678, A27
Jones G. C., Witstok J., Concas A., Laporte N., 2024, MNRAS, 529, L1
Kato Y. et al., 2018, PASJ, 70, L6
Kawamata R., Oguri M., Ishigaki M., Shimasaku K., Ouchi M., 2016, ApJ, 819, 114
Kerr A. R. et al., 2004, in Narayanan G., ed., Fifteenth International Symposium on Space Terahertz Technology. p. 55
Kerr A. R., Pan S.-K., Claude S. M. X., Dindo P., Lichtenberger A. W., Effland J. E., Lauria E. F., 2014, IEEE Trans. Terahertz Sci. Technol., 4, 201
Kirchschlager F., Schmidt F. D., Barlow M. J., Fogerty E. L., Bevan A., Priestley F. D., 2019, MNRAS, 489, 4465
Kirchschlager F., Sartorio N. S., De Looze I., Barlow M. J., Schmidt F. D., Priestley F. D., 2024, MNRAS, 528, 5364
Knudsen K. K., Watson D., Frayer D., Christensen L., Gallazzi A., Michałowski M. J., Richard J., Zavala J., 2017, MNRAS, 466, 138
Kohandel M., Pallottini A., Ferrara A., 2025, preprint (arXiv:2505.07935)
Kruijssen J. M. D., Longmore S. N., 2014, MNRAS, 439, 3239
Kruijssen J. M. D. et al., 2019, Nature, 569, 519
Langeroodi D., Hjorth J., Ferrara A., Gall C., 2024, preprint (arXiv:2410.14671)
Laporte N. et al., 2017, ApJ, 837, L21
Laporte N. et al., 2019, MNRAS, 487, L81
Le Fèvre O. et al., 2020, A&A, 643, A1
van Leeuwen I. F. et al., 2024, MNRAS, 534, 2062
Leśniewska A., Michałowski M. J., 2019, A&A, 624, L13
Liang L. et al., 2019, MNRAS, 489, 1397
Long A. S. et al., 2024, preprint (arXiv:2408.14546)
Lugaro M., Karakas A. I., Stancliffe R. J., Rijs C., 2012, ApJ, 747, 2
Ma Z. et al., 2024, ApJ, 975, 87
Mahieu S. et al., 2012, IEEE Trans. Terahertz Sci. Technol., 2, 29
Markov V., Gallerani S., Pallottini A., Sommovigo L., Carniani S., Ferrara A., Parlanti E., Di Mascia F., 2023, A&A, 679, A12
Markov V., Gallerani S., Ferrara A., Pallottini A., Parlanti E., Mascia F. D., Sommovigo L., Kohandel M., 2025, Nat. Astron., 9, 458
Martí-Vidal I., Vlemmings W. H. T., Muller S., Casey S., 2014, A&A, 563, A136
Matsuura M. et al., 2011, Science, 333, 1258
McKinney J., Cooper O. R., Casey C. M., Muñoz J. B., Akins H., Lambrides E., Long A. S., 2025, ApJ, 985, L21
McMullin J. P., Waters B., Schiebel D., Young W., Golap K., 2007, in Shaw R. A., Hill F., Bell D. J., eds, ASP Conf. Ser. Vol. 376, Astronomical Data Analysis Software and Systems XVI. Astron. Soc. Pac., San Francisco, p. 127
Meurer G. R., Heckman T. M., Calzetti D., 1999, ApJ, 521, 64
Michałowski M. J., 2015, A&A, 577, A80
Mitsuhashi I. et al., 2024a, A&A, 690, A197
Mitsuhashi I. et al., 2024b, ApJ, 971, 161
Morishita T. et al., 2023, ApJ, 947, L24
Narayanan D. et al., 2025, ApJ, 982, 7
Niculescu-Duvaz M. et al., 2022, MNRAS, 515, 4302
Novak M. et al., 2017, A&A, 602, A5
Oesch P. A. et al., 2016, ApJ, 819, 129
Overzier R. A. et al., 2011, ApJ, 726, L7
Pallottini A. et al., 2022, MNRAS, 513, 5621
Pallottini A., Ferrara A., Gallerani S., Sommovigo L., Carniani S., Vallini L., Kohandel M., Venturi G., 2025, A&A, 699, A6
Planck Collaboration VI, 2020, A&A, 641, A6
Popping G., Puglisi A., Norman C. A., 2017, MNRAS, 472, 2315
Pozzi F. et al., 2021, A&A, 653, A84
Prevot M. L., Lequeux J., Maurice E., Prevot L., Rocca-Volmerange B., 1984, A&A, 132, 389
Reddy N. A. et al., 2018, ApJ, 853, 56
Reuter C. et al., 2020, ApJ, 902, 78
Rihtaršič G. et al., 2024, A&A, 696, A15
Rowland L. E. et al., 2025, preprint (arXiv:2501.10559)
Sawicki M., 2012, PASP, 124, 1208
Saxena A. et al., 2024, preprint (arXiv:2411.14532)
Schaerer D., Boone F., Zamojski M., Staguhn J., Dessauges-Zavadsky M., Finkelstein S., Combes F., 2015, A&A, 574, A19
Schneider R., Maiolino R., 2024, A&AR, 32, 2
Schreiber C., Elbaz D., Pannella M., Ciesla L., Wang T., Franco M., 2018, A&A, 609, A30
Sekimoto Y., Iizuko Y., Satou N., Ito T., Kumagai K., Kamikura M., Naruse M., Shan W. L., 2008, in Wild W., ed., Nineteenth International Symposium on Space Terahertz Technology. p. 253
Smail I., Ivison R. J., Blain A. W., 1997, ApJ, 490, L5
Smith M. W. L. et al., 2017, ApJS, 233, 26
Sommovigo L., Algera H., 2025, MNRAS, 540, 3693
Sommovigo L., Ferrara A., Pallottini A., Carniani S., Gallerani S., Decataldo D., 2020, MNRAS, 497, 956
Sommovigo L., Ferrara A., Carniani S., Zanella A., Pallottini A., Gallerani S., Vallini L., 2021, MNRAS, 503, 4878
Sommovigo L. et al., 2022a, MNRAS, 513, 3122
Sommovigo L. et al., 2022b, MNRAS, 517, 5930
Sommovigo L. et al., 2025, ApJ, 990, 114
Spilker J. S. et al., 2023, Nature, 618, 708
Sugahara Y., Inoue A. K., Fudamoto Y., Hashimoto T., Harikane Y., Yamanaka S., 2022, ApJ, 935, 119
Takeuchi T. T., Yuan F.-T., Ikeyama A., Murata K. L., Inoue A. K., 2012, ApJ, 755, 144
Talia M., Cimatti A., Giulietti M., Zamorani G., Bethermin M., Faisst A., Le Fèvre O., Smolçić V., 2021, ApJ, 909, 23
Tamura Y. et al., 2019, ApJ, 874, 27
Tamura Y. et al., 2023, ApJ, 952, 9
Toyouchi D., Yajima H., Ferrara A., Nagamine K., 2025, MNRAS, 541, 3606
Tripodi R. et al., 2023, ApJ, 946, L45
Tsai C.-W. et al., 2015, ApJ, 805, 90
Tsukui T., Wisnioski E., Krumholz M. R., Battisti A., 2023, MNRAS, 523, 4654
Venemans B. P. et al., 2020, ApJ, 904, 130

Downloaded from https://academic.oup.com/mnras/article/544/2/1502/8318242 by guest on 21 November 2025

Viero M. P., Sun G., Chung D. T., Moncelsi L., Condon S. S., 2022, MNRAS, 516, L30
Vijayan A. P., Thomas P. A., Lovell C. C., Wilkins S. M., Greve T. R., Irodotou D., Roper W. J., Seeyave L. T. C., 2024, MNRAS, 527, 7337
Wang T. et al., 2019, Nature, 572, 211
Watson D., Christensen L., Knudsen K. K., Richard J., Gallazzi A., Michałowski M. J., 2015, Nature, 519, 327
Whitaker K. E., Pope A., Cybulski R., Casey C. M., Popping G., Yun M. S., 2017, ApJ, 850, 208
Witstok J., Jones G. C., Maiolino R., Smit R., Schneider R., 2023a, MNRAS, 523, 3119
Witstok J. et al., 2023b, Nature, 621, 267
Yung L. Y. A., Somerville R. S., Popping G., Finkelstein S. L., Ferguson H. C., Davé R., 2019, MNRAS, 490, 2855
Zavala J. A. et al., 2021, ApJ, 909, 165
da Cunha E. et al., 2013, ApJ, 766, 13
van der Vlugt D. et al., 2021, ApJ, 907, 5

APPENDIX A: BAND 9 OBSERVING CONDITIONS

Table A1 shows the parameters of the ALMA Band 9 observations. Band 9 was taken to characterize the dust temperature through a series of simulated observations of Y1 with potential dust temperatures between 60 and 120 K. Given the existing dust detections and upper-limits in Bands 5, 7, and 8, much deeper Band 8 (10 h at 410, 461 or 487 GHz) is unable to provide a robust dust temperature estimate, as it does not probe close enough to the peak to constrain the dust temperature accurately. Meanwhile four hours of Band 10 (at 870 GHz) is not sensitive enough to detect a dusty body at ≈ 70 K with high significance. This modelling further shows that Band 9 observations at 671 GHz are preferred relative to the slightly higher frequency option at 690 GHz, where the latter option has a slightly higher optical opacity.

Table A1. Parameters of the ALMA Band 9 observations.

UTC end time	Baseline length (m)	$N_{\rm ant}$	$T_{\rm int}$ (min)	PWV (mm)
2024-12-20 04:37:30	14–499	45	74.11	0.42
2024-12-13 06:04:48	14–313	44	73.10	0.59
2024-12-10 05:13:50	15–313	45	73.27	0.59
2024-11-09 05:06:37	14–313	43	74.42	0.34

Note. Col. 1: UTC end time of the observations as [YYYY-MM-DD hh:mm:ss]. Col. 2: length between the nearest and furthest antennae. Col. 3: number of antennae participating in the observations. Col. 4: the total observation time including overheads. Col. 5: the precipitable water vapour during the observations.

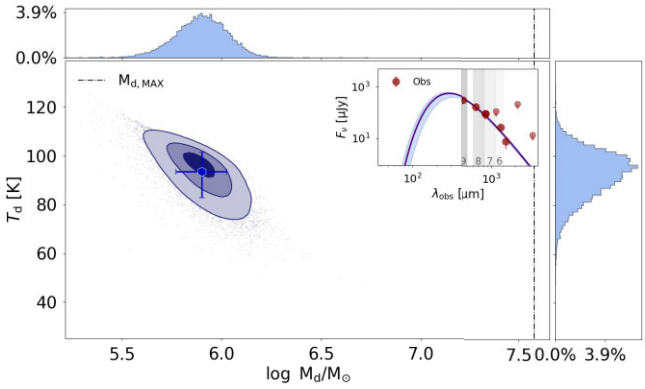

Figure B1. Recovered distribution of $T_{\rm d,[C\,II]}$ as a function of dust mass for Y1 using the updated fluxes detailed in Table 1. The resulting dust temperature (94^{+8}_{-11} K) and dust mass ($8.0^{+2.6}_{-2.0} \times 10^5$ M$_\odot$) broadly agree with the direct fitting results. The contours show the 16$^{\rm th}$, 50$^{\rm th}$, and 84$^{\rm th}$ percentiles of the distribution, with the median value represented by the purple square. The best-fitting spectrum, also shown in *black dashed lines* in Fig. 2, is shown in the inset, together with all data and upper limits.

APPENDIX B: [C II]-BASED DUST TEMPERATURE ESTIMATE

Using the methodology detailed in L. Sommovigo et al. (2021), a refit of Y1 is made using the Band 7 continuum flux of 137 ± 26 μJy at 353 GHz. Using the updated stellar mass from *JWST* imaging of 10^9 M$_\odot$, as well as a characteristic [C II] size between once and twice that of the stellar emission (Bakx et al. in prep.), a dust fit is performed in Fig. B1. The resulting dust temperature is 94^{+8}_{-11} K, with a total dust mass of $8.0^{+2.6}_{-2.0} \times 10^5$ M$_\odot$, similar to those from the direct SED fit shown in Fig. 2.

APPENDIX C: *JWST* DATA FOR $\beta_{\rm UV}$ CALCULATION

Fig. C1 shows the compilation of *JWST* data used for calculating the spatially resolved $\beta_{\rm UV}$ values. The combined red–green–blue (rgb) image of Y1 is shown in Fig. C2.

Downloaded from https://academic.oup.com/mnras/article/544/2/1502/8318242 by guest on 21 November 2025

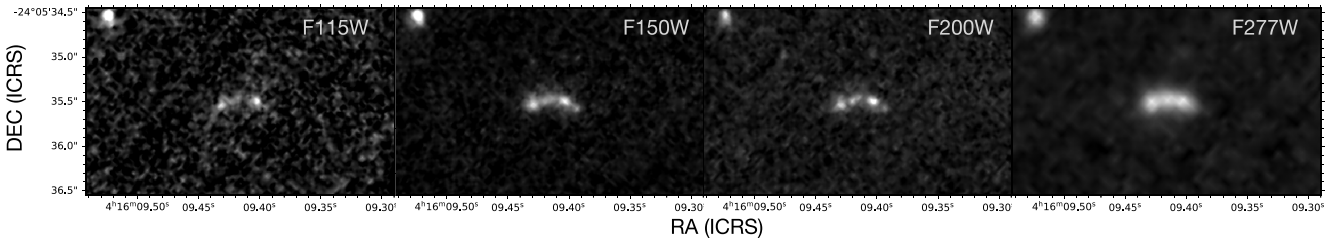

Figure C1. The *JWST* photometric images in filters *F115W*, *F150W*, *F200W*, and *F277W*. The latter three are used for the $\beta_{\rm UV}$ analysis, after smoothing everything to the resolution of *F277W*.

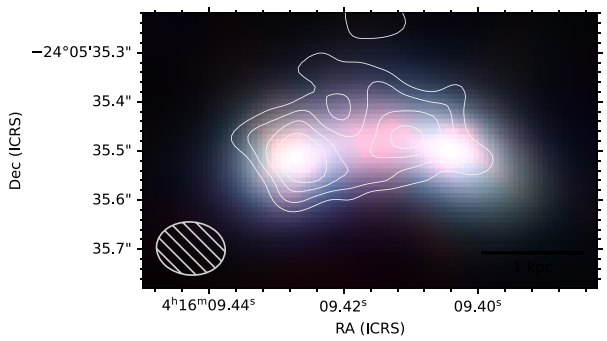

Figure C2. The combined *JWST* photometric images in filters *F150W* (b), *F200W* (g), and *F277W* (r).

[1]*Department of Space, Earth and Environment, Chalmers University of Technology, SE-412 96 Gothenburg, Sweden*
[2]*Center for Computational Astrophysics, Flatiron Institute, 162 5th Avenue, New York, NY 10010, USA*
[3]*Department of Physics, Graduate School of Science, Nagoya University, Aichi 464-8602, Japan*
[4]*Astrophysics Research Institute, Liverpool John Moores University, 146 Brownlow Hill, Liverpool L3 5RF, UK*
[5]*Scuola Normale Superiore, Piazza dei Cavalieri 7, I-56126 Pisa, Italy*
[6]*Institute of Astronomy and Astrophysics, Academia Sinica, 11F of Astronomy-Mathematics Building, No.1, Section 4, Roosevelt Rd, Taipei 106319, Taiwan, R.O.C.*
[7]*Institute of Physics of Rennes, UMR-CNRS 6251, University of Rennes, F-35000 Rennes, France*
[8]*Division of Physics, Faculty of Pure and Applied Sciences, University of Tsukuba, Tsukuba, Ibaraki 305-8571, Japan*
[9]*Tomonaga Center for the History of the Universe (TCHoU), Faculty of Pure and Applied Sciences, University of Tsukuba, Tsukuba, Ibaraki 305-8571, Japan*
[10]*National Astronomical Observatory of Japan, 2-21-1 Osawa, Mitaka, Tokyo 181-8588, Japan*
[11]*Department of Astronomical Science, The Graduate University for Advanced Studies, SOKENDAI, 2-21-1 Osawa, Mitaka, Tokyo 181-8588, Japan*
[12]*Institute of Astronomy, Graduate School of Science, The University of Tokyo, 2-21-1 Osawa, Mitaka, Tokyo 181-0015, Japan*
[13]*Instituto de Física y Astronomía, Universidad de Valparaíso, Avda. Gran Bretaña 1111, Valparaíso, Chile*
[14]*Millenium Nucleus for Galaxies (MINGAL), Avda. Gran Bretaña 1111, Valparaíso, Chile*
[15]*Hiroshima Astrophysical Science Center, Hiroshima University, 1-3-1 Kagamiyama, Higashi – Hiroshima, Hiroshima 739-8526, Japan*
[16]*Department of Physics, School of Advanced Science and Engineering, Faculty of Science and Engineering, Waseda University, 3-4-1 Okubo, Shinjuku, Tokyo 169-8555, Japan*
[17]*Waseda Research Institute for Science and Engineering, Faculty of Science and Engineering, Waseda University, 3-4-1 Okubo, Shinjuku, Tokyo 169-8555, Japan*
[18]*Aix Marseille Université, CNRS, CNES, LAM (Laboratoire d'Astrophysique de Marseille), UMR 7326, F-13388 Marseille, France*
[19]*Department of Pure and Applied Physics, School of Advanced Science and Engineering, Faculty of Science and Engineering, Waseda University, 3-4-1 Okubo, Shinjuku, Tokyo 169-8555, Japan*
[20]*Department of Chemistry and Molecular Biology, University of Gothenburg, SE-413 90, Gothenburg, Sweden*
[21]*Department of Cosmosciences, Graduate School of Science, Hokkaido University, N10W8, Kitaku, Sapporo 060-0810, Japan*
[22]*Dipartimento di Fisica 'Enrico Fermi', Universitá di Pisa, Largo Bruno Pontecorvo 3, Pisa I-56127, Italy*
[23]*Institute for Advanced Research, Nagoya University, Furocho, Chikusa, Nagoya 464-8602, Japan*

This paper has been typeset from a TEX/LATEX file prepared by the author.

Downloaded from https://academic.oup.com/mnras/article/544/2/1502/8318242 by guest on 21 November 2025

© The Author(s) 2025.
Published by Oxford University Press on behalf of Royal Astronomical Society. This is an Open Access article distributed under the terms of the Creative Commons Attribution License (https://creativecommons.org/licenses/by/4.0/), which permits unrestricted reuse, distribution, and reproduction in any medium, provided the original work is properly cited.